Automated detection method for architectural distortion areas on mammograms based on morphological processing and surface analysis

Tetsuko ICHIKAWA[*a], Tomoko MATSUBARA[b], Takeshi HARA[a], Hiroshi FUJITA[a], Tokiko ENDO[c], Takuji IWASE[d]

[a]Department of Intelligent Image Information, Division of Regeneration and Advanced Medical Science, Graduated School of Medicine, Gifu University, 1-1 Yanagido, Gifu, 501-1193 Japan
[b]Department of Information Culture, School of Information Culture, Nagoya Bunri University, 365 Maeda, Inazawa-cho, Inazawa, 492-8520 Japan
[c]Department of Radiology, National Hospital of Nagoya, 4-1-1 Sannomaru, Naka-ku, Nagoya, 460-0001 Japan
[d]Cancer Institute Hospital, 1-37-1 Kamiikebukuro, Toshima-ku, Tokyo, 170-8455 Japan

ABSTRACT

As well as mass and microcalcification, architectural distortion is a very important finding for the early detection of breast cancer via mammograms, and such distortions can be classified into three typical types: spiculation, retraction, and distortion. The purpose of this work is to develop an automatic method for detecting areas of architectural distortion with spiculation. The suspect areas are detected by concentration indexes of line-structures extracted by using mean curvature. After that, discrimination analysis of nine features is employed for the classifications of true and false positives. The employed features are the size, the mean pixel value, the mean concentration index, the mean isotropic index, the contrast, and four other features based on the power spectrum. As a result of this work, the accuracy of the classification was 76% and the sensitivity was 80% with 0.9 false positives per image in our database in regard to spiculation. It was concluded that our method was effective in detectiong the area of architectural distortion; however, some architectural distortions were not detected accurately because of the size, the density, or the different appearance of the distorted areas.

Keywords: architectural distortion, mammogram, computer-aided diagnosis

1. INTRODUCTION

Recently, the incidence rate of breast cancer has been increasing rapidly due to the westernization of Japan's life style. Breast cancer has been reported to have the highest mortality rate of any women's cancer. Mammography is currently the most effective way for detecting early stage of breast cancer. However, mammograms are not easily interpreted, especially by inexperienced radiologists in screening situations. Therefore, it is necessary to develop a computer-aided diagnosis (CAD) to provide a second opinion to radiologists in order to reduce the number of false-negative readings and to help them diagnose mammograms more efficiently. Many different techniques have been developed to detect masses and microcalcifications automatically, and several companies have successfully commercialized CAD systems.

Behind masses and microcalcifications, architectural distortion is the third most common mammographic finding of breast cancer. Architectural distortions appear as spiculation, retraction, and distortion. Although most architectural distortions must be considered to represent cancer, it is difficult for radiologists to detect them because their manifestations are frequently subtle.[1] However, fewer than one half of the cases of architectural distortion were detected by the two most widely available CAD systems.[2] Therefore, development of CAD system for detecting architectural distortions is valuable.

Our current detection method for masses[3,4] is able to detect a certain type of architectural distortion, but the sensitivity is low. We have also developed a detection method for spiculation based on a multistage pendulum filter.[5] This method was not able to allow us to detect architectural distortions because this filter is applied to the detected mass candidates.

Medical Imaging 2004: Image Processing, edited by J. Michael Fitzpatrick, Milan Sonka, Proceedings of SPIE Vol. 5370 (SPIE, Bellingham, WA, 2004)
1605-7422/04/$15 doi: 10.1117/12.535116

We have been developing a detection method for architectural distortions with focal retraction based on morphological processing.[6, 7, 8] It indicated high sensitivity but it was necessary to add another detection algorithm for architectural distortions without retraction. The purpose of this study is to develop a new detection method for the area of architectural distortion with spiculation in order to improve detection performance.

2. METHODS

Figure 1 shows two typical types of architectural distortions. (b) is an image with spiculation, and (d) is an image with focal retraction. The detection target of this method is the spiculation area as shown in (b). Each step of our detection method is explained below.

2.1 Image digitization

All of the screen/film mammograms are digitized by using the Konica LD-5500 laser digitizer at 0.05 mm pixel size with 12-bit density resolution. Digital mammograms are subsampled to an effective pixel size of 0.4 mm for the detection of architectural distortions.

(a) (b) (c) (d)

Fig. 1. Examples of two typical types of architectural distortions. (a) Architectural distortion with speculation. (c) Architectural distortion with focal retraction. The sketches drawn by a radiologist are shown in (b) and (d), respectively.

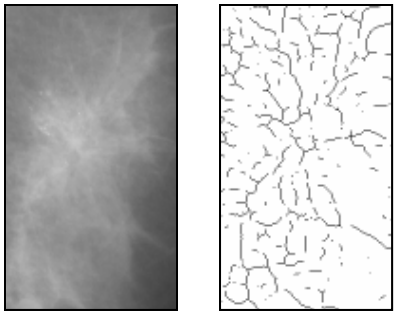

(a) (b)

Fig. 2. An example of detection of line-structure.
(a) An original image. (b) Detected line-structure image.

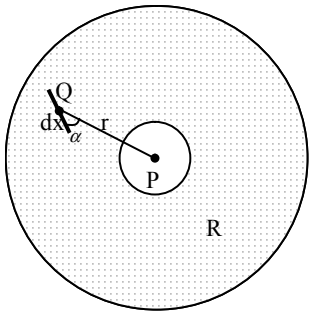

Fig. 3. A concentration index filter.

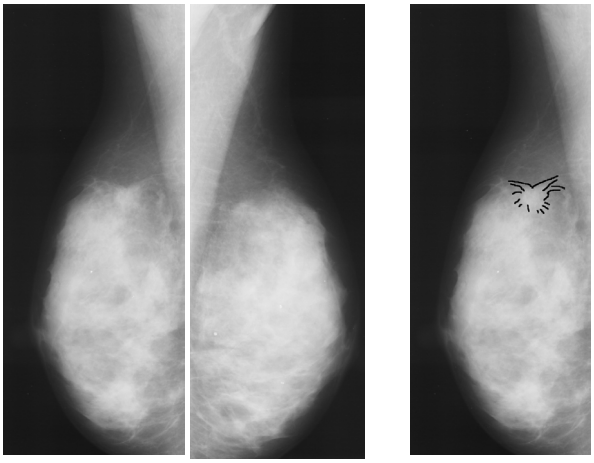

(a) (b)

Fig. 4. An example of architectural distortion detected based on half-circle concentration index.

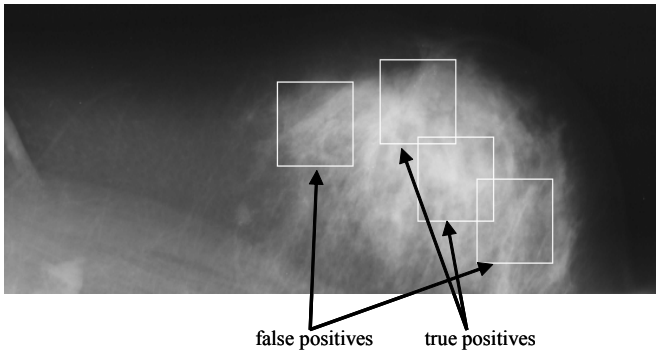

Fig. 5. An example of selected ROI.

2.2 Detection of suspect regions

2.2.1 Detection of line-structure

The sign of the mean curvature represents the surface direction.[9, 10] The pixel value of the mammary gland is smaller than that of the surrounding region, so the sign of the mean curvature at the mammary gland is positive. The quadric surface $z = h(x, y)$ is assigned to point P and its 13×13 neighborhood pixels by the least-squares method. z axis is a pixel value. Here, mean curvature H is given by

$$H = \frac{(1+h_x^2)h_{yy} + (1+h_y^2)h_{xx} - 2h_x h_y h_{xy}}{2(1+h_x^2+h_y^2)^{3/2}} \quad (1)$$

In Eq. (1), h_x shows $\partial h(x,y)/\partial x$, and h_{xx} shows $\partial^2 h(x,y)/\partial x \partial x$. Figure 2 shows an example of the detected line-structure. The line-structure corresponds to the mammary gland.

2.2.2 Calculation of the concentration index[11, 12]

In the first step, line primitives are assigned to connecting points of the line-structure detected by the surface analysis. The length of the line primitive is half of the length of the line connecting the anteroposterior points, and its orientation is the same. Let us denote the pixel of interest at (x, y) by P. The region of support R is shown in Figure 3. P is not included in R. The concentration index at point P is given as follows:

$$C(P) = \frac{\Sigma_R(dx|\cos\alpha|/r)}{\Sigma_R(dx/r)}, \quad (2)$$

where dx is the length of line primitive Q, r is the distance between P and Q, and α refers to the orientation of Q with respect to the line PQ. Σ_R shows the total of all line primitives in region R. When no line primitive in R, the concentration index is defined as 0. The suspect regions correspond to the high concentration regions. The concentration index in the region of the half-circle is used in order to detect the architectural distortion with retraction as shown in Figure 4. The maximum value is selected from the concentration indexes extracted with the diverse angle half-circles.

2.3 Elimination of false positives

Nine features are extracted, and the discrimination analysis is employed.

The size of the ROI is a 512×512 square region centralized on the suspect region as shown in Figure 5. The ROI is used in order to extract the feature values (6) ~ (9) below. Each feature is explained in the following.

(1): The size of the suspected region.

(2): The mean pixel value of the suspected region. That of the architectural distortion area is generally low.

(3): The mean concentration index of the suspected region.

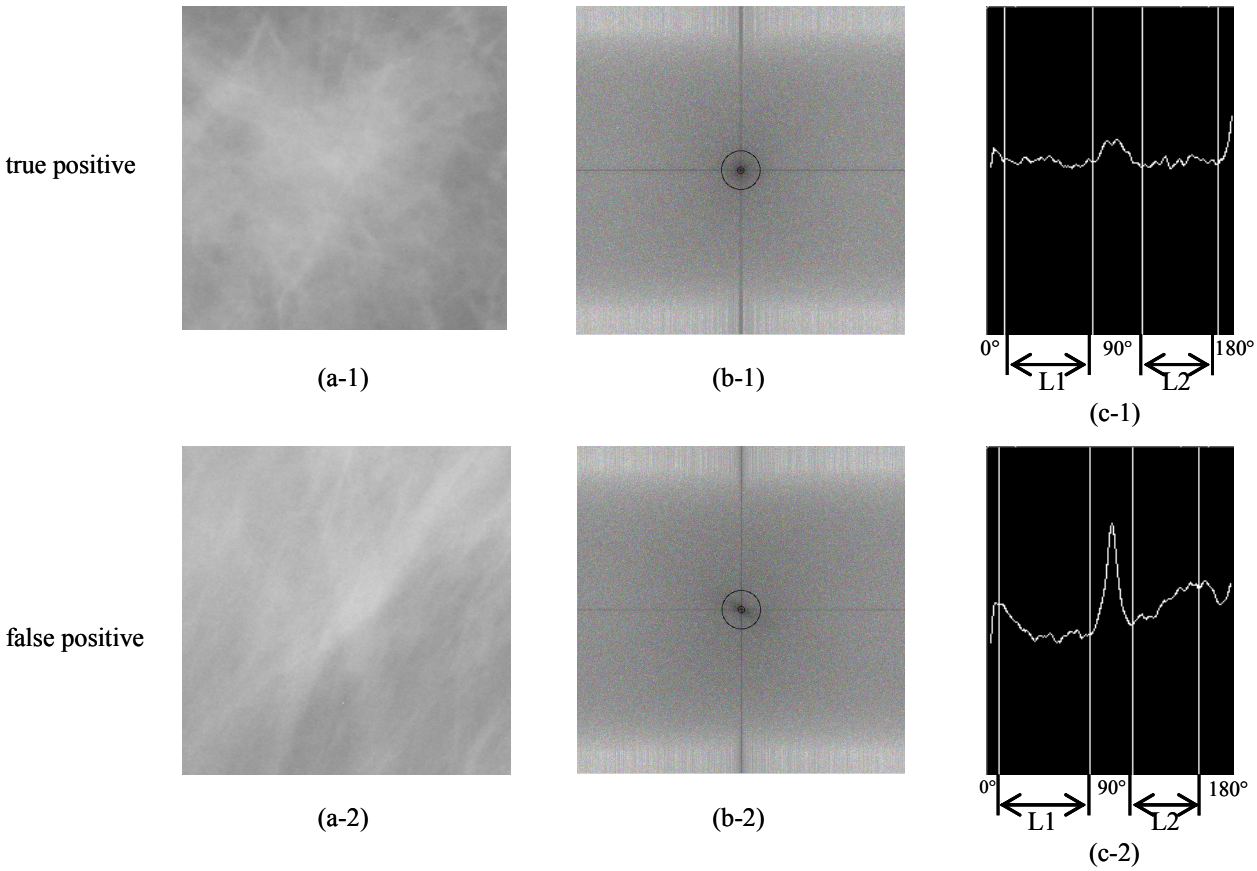

Fig. 6. Images of power spectra (b-1) and (b-2), and their profiles (c-1) and (c-2) of typical true positive (a-1) and false positive (a-2), respectively. (a-1) and (a-2) are images of selected ROI.

(4): The isotropic index[11, 12] shows the variation in the concentration indexes of small regions of R. The isotropic index can be high when the line-structure exists in all directions as does the region of architectural distortion. On the other hand, the isotropic index of the blood vessel regions can be low, because they have line-structures from particular directions.

(5): The contrast between the suspected region and surrounding region.

(6) and (7): Figures 6 (b-1) and (b-2) show the power spectra of typical true positive and false positive, respectively, which are obtained from the two-dimensional Fourier transforms. Observing these images, we find that the intensity variations are different. The variation of the typical false positive is more evident than that of the typical true positive. The rings in Figures 6 (b-1) and (b-2) show the band-pass filter. The root-mean-square variation R and the first moment of the power spectrum M are defined as follows: [13]

$$R = \sqrt{\sum_{u=1}^{n}\sum_{v=1}^{n}\left|T(u,v)\right|^2} \qquad (3)$$

$$M = \frac{\sum_{u=1}^{n}\sum_{v=1}^{n}\sqrt{u^2+v^2}\left|T(u,v)\right|^2}{\sum_{u=1}^{n}\sum_{v=1}^{n}\left|T(u,v)\right|^2} \quad , \quad (4)$$

where n and $T(u,v)$ correspond to the matrix size and the Fourier transform of the texture, respectively. R and M are determined as quantitative measures of the magnitude and the coarseness (or fineness) of the texture.

(8) and (9): Figures 6 (c-1) and (c-2) show the results of profiling the power spectra in the rings as shown in Figures 6 (b-1) and (b-2) at each angle from 0 degrees to 180 degrees. A typical false positive has a peak at the right angle to the texture direction. On the other hand, a typical true positive has no peak. First, the peaks around 0, 90, and 180 degrees are eliminated in order to detect the difference of profiles. The vertical lines in Figures 6 (c-1) and (c-2) show the results of the peak elimination. The area between 0 and 90 degrees and the area between 90 and 180 degrees without peaks at around 0, 90, and 180 degrees are defined as L1 and L2, respectively. Second, the difference between the L1 average and L2 average is selected as feature (8). Finally, a linearization is performed to L1 and L2. Feature (9) is the difference of the slope magnitude between L1 and L2.

Discrimination analysis is performed by using the above nine features. The round robin method is also used to estimate the performance, because our database is small.

3. RESULTS AND DISCUSSION

Our image database of architectural distortions consists of 94 images. Forty-one images have architectural distortions with spiculations. After the detection of suspected regions, the sensitivity was 92% (38/41) and the number of false positives per image was 3.3(136/41). Three undetected images were classified into category 3 (probably benign) by radiologists because they are small or low density. Table 1 shows the result of discrimination analysis for 165 suspect regions (true positive: 58, false positive: 107). The accuracy of the discrimination analysis was 76% and the sensitivity was 80% (33/41) with 0.9 (35/41) false positives per image in our database in regard to spiculation. The major causes of misclassification are false positives similar to true positives and deviation of the suspect region position from the center of the architectural distortion. The sensitivity was 56% (53/94) with 1.0 (91/94) false positives per image for all images. It is possible to detect two architectural distortions by adding the detection method with a half-circle concentration index.

The method for detecting architectural distortion with retraction achieved a sensitivity of 92% (12/13) with 2.5 (32/13) false positives per image in intended cases[6, 7, 8]. Combining these two methods, the sensitivity was 68% (64/94) with 3.4 (316/94) false positives per image for all images. Neither retraction nor spiculation exists in some undetected architectural distortions.

Table 1 Result of discrimination analysis.

correct class	classified class	
	TP	FP
TP	50	12
FP	35	101

4. CONCLUSIONS

We have developed an automated method to detect the area of architectural distortion with spiculation. The high sensitivity of our approach indicates that our method will be useful, although some of them were not detected correctly. For the future work, it is necessary to decrease the number of false positives and to add the detection method for the architectural distortions undetected by our method.

ACKNOWLEDGMENTS

This work was supported in part by the Ministry of Health, Labour and Welfare under a Grant-In-Aid for Cancer Research, in part by the Ministry of Education, Culture, Sports, Science and Technology under a Grant-In-Aid for Scientific Research from the Japanese Government, and in part by Daiwa Securities Health Foundation.

REFERENCES

1. Y. Hatanaka, T. Matsubara, T. Hara, N. Shinohara, D. Fukuoka, H. Fujita and T. Endo, "A comparison between physicians' interpretation and a CAD system's cancer detection by using a mammogram database in a physicians' self-learning course", *Jpn. J. Radiol. Technol.*, vol.58, no.3, pp.375-382, 2000, in Japanese
2. J. A. Baker, E. L. Rosen, J. Y. Lo, E. I. Gimenez, R. Walsh, and M. S. Soo, "Computer-Aided Detection (CAD) in Screening Mammography: Sensitivity of Commercial CAD Systems for Detecting Architectural Distortion", *AJR 181* pp.1083-1088, 2003.
3. T. Matsubara, H. Fujita, S. Kasai, O. Otsuka, T. Hara and T. Endo, "Development of a new algorithm for detection of mammographic masses," *in Proc. of the 4th International Workshop on Digital Mammotraphy, in DIGITAL MAMMOGRAPHY '98*, pp.139-142, Elsevier Science, 1998.
4. S. Kasai, D. Kaji, A. Kano, H. Fujita, T. Hara and T. Endo, "Mass detection algorithm for digital mammograms based on an adaptive thresholding technique utilizing multi-resolution processing", *in Proc. of the 6th International Workshop on Digital Mammography, in DIGITAL MAMMOGRAPHY*, pp.334-338, Springer, 2002.
5. M. Goto, A. Morishita, H. Fujita, T. Hara and T. Endo, "Detection of spicules on mammograms based on a multistage pendulum filter", *in Proc. of the 4th International Workshop on Digital Mammography, in DIGITAL MAMMOGRAPHY '98*, pp.135-138, Elsevier Science, 1998.
6. D. Yamazaki, T. Matsubara, H. Fujita, T. Hara, T. Endo, and T. Iwase, "Automated extraction method for region of architectural distortion on mammograms", *Med. Imag. and Inform. Sci.*, vol. 19, no. 2, pp.69-72, 2002, in Japanese
7. T. Matsubara, D. Yamazaki, T. Hara, H. Fujita, S. Kasai, T. Endo, and T. Iwase, "Automated detection of architectural distortions on mammograms", *in Proc. of IWDM2002-6th International Workshop on Digital Mammography*, pp.350-352, Springer publishing, 2002.
8. T. Matsubara, T. Ichikawa, T. Hara, H. Fujita, S. Kasai, T. Endo, and T. Iwase, "Automated detection methods for architectural distortions around skinline and within mammary gland on mammograms", *in Proc. of CARS2003 – Computer Assisted Radiology and Surgery*, pp.950-955, Elsevier, 2003.
9. O. Monga and S. Benayoun, "Using Partial Derivatives of 3D Images to Extract Typical Surface Features", *Computer Vision and Image Understanding*, vol. 61, no.2, pp.171-189, March. 1995.
10. J. P. Thirion and A. Gourdon, "Computing the Differential Characteristics of Isointensity Surfaces", *Computer Vision and Image Understanding*, vol. 61, no.2, pp.190-202, March. 1995.
11. J. Hasegawa, T. Tsutsui, and J. Toriwaki, "Automated Extraction of Cancer Lesions with Convergent Fold Patterns in Double Contrast X-Ray Images of Stomach", The IEICE Transactions on Information and Systems, PT.2 (Japanese Edition), vol.J73-D- Ц no.4, pp.661-669, April 1990. in Japanese
12. K. Mekada, K. Oza, J. Hasegawa, and J. Toriwaki, "Features of Local Concentration Patterns in Line Figures and Their Applications", The IEICE Transactions on Information and Systems, PT.2 (Japanese Edition), vol.J77-D- Ц no.9, pp.1788-1796, Sep.1994. in Japanese
13. S. Katsuragawa, K. Doi, N. Nakamori, and H. MacMahon, "Image feature analysis and computer-aided diagnosis in digital radiography: Effect of digital parameters on the accuracy of computerized analysis of interstitial disease in digital chest radiographs," *Med. Phys.*, 17(1), Jan/Feb 1990.

*ichikawa@fjt.info.gifu-u.ac.jp; phone +81-58-293-2746; fax +81-58-230-1895; www.fjt.info.gifu-u.ac.jp